ELSEVIER

Materials Science and Engineering A324 (2002) 77–81

MATERIALS SCIENCE & ENGINEERING A

www.elsevier.com/locate/msea

In-situ neutron scattering studies of order and decomposition in Ni-rich Ni–Ti☆

R. Bucher [a], B. Demé [b], H. Heinrich [a], J. Kohlbrecher [c], M. Kompatscher [a], G. Kostorz [a,*], J.-M. Schneider [a], B. Schönfeld [a], M. Zolliker [c]

[a] *ETH Zürich, Institute of Applied Physics, CH-8093 Zürich, Switzerland*
[b] *Institut Laue-Langevin, F-38042 Grenoble, France*
[c] *Paul Scherrer Institut, CH-5232 Villigen PSI, Switzerland*

Abstract

Diffuse wide-angle neutron scattering experiments have been performed for two states of thermal equilibrium within the γ solid solution, ^{58}Ni–5.8 at.% Ti at 777 K and ^{58}Ni–9.6 at.% Ti at 1103 K. The analysis of the Clapp configurations yields the basic cluster of the $L1_2$ structure as the most important local configuration. Neither the static nor the dynamic atomic displacements indicate any precursor of the stable hexagonal phase ($D0_{24}$ structure) containing 25 at.% Ti. Metastable states with precipitates showing non-stoichiometric $L1_2$ structure evolve during the decomposition of supersaturated Ni–11.3 at.% Ti polycrystals as seen by in-situ small-angle neutron scattering. From the integrated small-angle scattering intensity, the Ti content of the cuboidally shaped precipitates in the metastable γ″ state is found to be about 17 at.% between 870 and 950 K.

Keywords: Small-angle scattering; Wide-angle diffuse scattering; Short-range order; Metastable states; Ni–Ti alloys

1. Introduction

Supersaturated solid solutions of Ni-rich Ni–Ti show some particularly complex aspects of phase separation. Various methods like atom-probe field-ion microscopy, transmission electron microscopy, magnetic measurements, X-ray diffraction and more recently neutron diffraction have been employed to analyse the decomposition path, with partly contradictory results on the interplay of order and decomposition. Results of X-ray measurements by Hashimoto and Tsujimoto [1] led to the introduction of a metastable miscibility gap of the γ″ state and the position of various thermodynamic lines was discussed by Soffa and Laughlin [2]. Coherent precipitates of cuboidal shape, aligned along the elastically soft ⟨100⟩ direction and having $L1_2$ type of order evolve first. Two metastable states (γ″ and γ′ with a different non-stoichiometry of the precipitates (Fig. 1)) were identified before the stable η phase evolves [3–6]. The structure of the η phase ($D0_{24}$) is closely related to $L1_2$ as the site occupation by Ni and Ti in hexagonal basal planes and {111} fcc planes is the same.

In this paper results from neutron scattering are presented. This research (see Refs [3–6,9] for previous results) benefits from the excellent scattering contrast of Ni and Ti for neutrons. The appearance of the metastable γ″ state in Ni–Ti is monitored by in-situ small-angle neutron scattering (SANS). The structure of the precipitates is related to the microstructure within the γ solid solution investigated by diffuse wide-angle scattering. Effective atomic interactions can be determined from the diffuse scattering of samples in thermal equilibrium [10,11], and indications may also be obtained for the structure of metastable states as long as they are based on a coherent lattice.

☆ This paper is dedicated to Professor P. Lukáč on the occasion of his 65th birthday.

* Corresponding author. Tel.: +41-1-6333399; fax: +41-1-6331105.
E-mail address: kostorz@iap.phys.ethz.ch (G. Kostorz).

0921-5093/02/$ - see front matter
PII: S0921-5093(01)01287-4

2. Experiment

Samples of ^{58}Ni–5.8 at.% Ti and ^{58}Ni–9.6 at.% Ti of cylindrical shape (diameter of 9 mm, about 10 mm in height) were cut by spark erosion from single crystals grown by the Bridgman method. The isotope ^{58}Ni was used to enhance the scattering contrast and to eliminate the large elastic incoherent scattering of natural Ni. States of thermal equilibrium within the γ solid solution were investigated by diffuse wide-angle neutron scattering, at room temperature for a state quenched-in from 777 K (Ni–5.8 at.% Ti), and in situ at 1103 K (Ni–9.6 at.% Ti). Measurements were performed in the elastic mode on the triple-axis spectrometer IN3 (ILL, Grenoble) equipped with an Eulerian cradle and a furnace [9]. For both alloys, the diffuse scattering was measured at about 2000 positions within the minimum separation volume close to the direct beam, using neutrons of a wavelength of 0.236 and 0.153 nm. The incoherent scattering from a polycrystalline vanadium sample served to convert diffuse scattering intensities to absolute scattering cross-sections.

Polycrystals of Ni–10.1 and 11.3 at.% Ti with an average grain size of about 0.5 mm were obtained from swaging two as-cast rods from 16 to 12 mm in diameter and aging them at 1470 K for 1 h and for 24 h at 900 K. Slices, about 3.5 mm in thickness, were homogenized at 1470 K for 2 h and quenched in water. The homogeneity of the slices was within 0.1 at.% Ti. The aging was monitored in situ in the neutron beam at the SANS instrument of the Paul Scherrer Institut, Villigen, Switzerland. Neutrons of an average wavelength $\lambda = 0.8$ nm (wavelength resolution of 10%) were used to avoid double-Bragg scattering from precipitates with $L1_2$ structure. A new high-temperature furnace was employed in the most recent investigations allowing the homogenized samples to be brought to the annealing temperature between 870 and 950 K within 1 min (before: 5 min). Data were taken for a Q range from 0.1 to 1.9 nm^{-1} (Q is the modulus of the scattering vector, $Q = 4\pi \sin\theta/\lambda$ where θ = half the scattering angle) for 1 to 4 d and calibrated by the incoherent scattering of a vanadium single crystal.

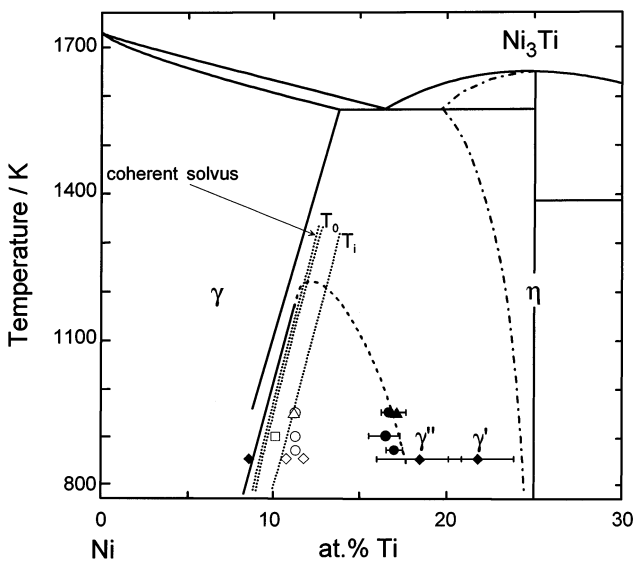

Fig. 1. Ni-rich part of the Ni–Ti phase diagram [7] with the modification given by Bellen et al. [8] for the η phase. The coherent solvus, the equilibrium line T_0 and the ordering instability line T_i (dotted lines) introduced by Soffa and Laughlin [2] and calculated with the EPI parameters of [9] are shown together with the metastable miscibility gap suggested by [1]. Open symbols indicate the starting states of supersaturated solid solutions, filled symbols the concentrations of matrix and precipitates for the γ'' state ([4,5] and this work).

3. Short-range order in the γ solid solution

The elastic coherent diffuse wide-angle scattering $I_{\mathrm{diff}}(\underline{h})$ consists of short-range order $I_{\mathrm{SRO}}(\underline{h})$, size-effect $I_{\mathrm{SE}}(\underline{h})$ and Huang $I_{\mathrm{H}}(\underline{h})$ scattering:

$$I(\underline{h}) = Nc_{\mathrm{Ni}}c_{\mathrm{Ti}}|b_{\mathrm{Ni}} - b_{\mathrm{Ti}}|^2[I_{\mathrm{SRO}}\,(\underline{h}) + I_{\mathrm{SE}}\,(\underline{h}) + I_{\mathrm{H}}(\underline{h})] \quad (1)$$

where $\underline{h} = (h_1, h_2, h_3)$ is the scattering vector $\underline{Q}$ in reciprocal lattice units ($\underline{h} = \underline{Q}/(2\pi/a)$, a = lattice parameter), c_{Ni}, c_{Ti} are the atomic fractions, b_{Ni}, b_{Ti} the coherent scattering lengths and N is the number of atoms. The prefactor $c_{\mathrm{Ni}}c_{\mathrm{Ti}}|b_{\mathrm{Ni}} - b_{\mathrm{Ti}}|^2$ is called one Laue unit per atom. The three scattering contributions comprise a total of ten Fourier series with:

$$I_{\mathrm{SRO}}(\underline{h}) = \textstyle\sum_{lmn}\alpha_{lmn}\cos(\pi h_1 l)\cos(\pi h_2 m)\cos(\pi h_3 n). \quad (2)$$

The α_{lmn} are the Warren–Cowley short-range order parameters of neighborhood shell lmn (l, m, n, in units of $a/2$). For further details, see, for example, Refs. [10,11].

The scattering contributions were separated by a least-squares fitting procedure with the dominant Fourier coefficients. The recalculated short-range order scattering (about 30 shells were considered) is shown in Fig. 2. Diffuse maxima are seen at 100 positions, the location of the $L1_2$ superstructure reflections. Lines of equal intensity close to the 100 positions are of more spherical than ellipsoidal shape. This fact may reflect a lower tendency for the formation of antiphase boundaries on {100} planes, in contrast to, for example, Ni-rich Ni–Al [11], and may be related to the metastability of the $L1_2$ structure as Ti–Ti nearest neighbors will then be avoided in the subsequent $L1_2$ to $D0_{24}$ transformation.

This conclusion is supported by a configurational analysis in terms of Clapp configurations [12] that was performed for modelled crystals ($32 \times 32 \times 32$ fcc unit cells) consistent with the sets of Warren–Cowley short-range order parameters α_{lmn}. In such an analysis all

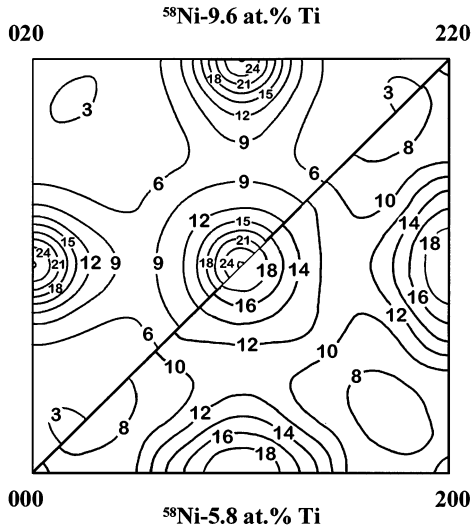

Fig. 2. Recalculated short-range order scattering I_{SRO} for the 001 plane in 0.1 Laue units of ^{58}Ni–5.8 at.% Ti (state at 777 K) and ^{58}Ni–9.6 at.% Ti (at 1103 K).

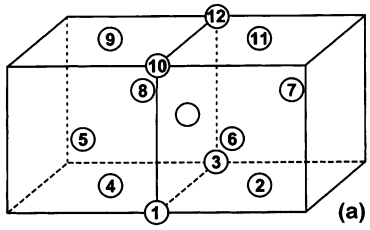

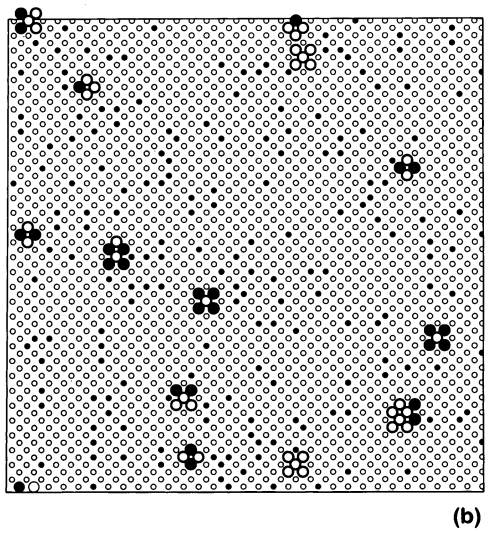

Fig. 3. Local atomic arrangements in fcc alloys. (a) Coordination polyhedron of the 110 shell. (b) A (100) plane of a modelled crystal of ^{58}Ni–9.6 at.% Ti (1103 K), with Ni atoms (open circles) and Ti atoms (filled circles). Atoms within this plane that belong to a C16 or C17 Clapp configuration are marked by large symbols (atoms in adjacent planes complete these clusters).

nearest-neighbor configurations are systematically searched and their abundance enhancement with respect to a statistically uncorrelated arrangement of identical average composition is determined. Local elements with a large enhancement are considered to indicate, plausible stable or metastable structures (Fig. 3). For the case of Ti atoms around a Ni atom the important clusters are the C16 (only sites 5,6,7,8 in Fig. 3a — or symmetrically equivalent arrangements — are occupied by Ti, the others by Ni) and the C17 Clapp configurations (only sites 4,6,7,9 are occupied by Ti). Configuration C16 is the basic cluster of the $L1_2$ structure, while C17 arises if antiphase boundaries are introduced in the $L1_2$ structure (as, for example, in $D0_{22}$ and $D0_{23}$). Configuration C17 is less enhanced (factors are 2.9 (C17) and 26 (C16) for ^{58}Ni–5.8 at.% Ti, 5.3 (C17) and 20 (C16) for ^{58}Ni–9.6 at.% Ti) than for systems with a stable $L1_2$ structure like Ni–Al [3.0 (C17) and 7.0 (C16)], see Ref. [11].

As short-range order was determined for states of thermal equilibrium, effective pair interaction (EPI) parameters $V_{lmn} = (V^{AA}_{lmn} + V^{BB}_{lmn} - 2V^{AB}_{lmn})/2$ can be determined that enter the ordering energy $\Delta E_{ord} = Nc_{Ni}c_{Ti}\Sigma_{lmn}V_{lmn}\alpha_{lmn}$ (with $lmn \neq 000$). The inverse Monte Carlo method [13] as well as the Krivoglaz–Clapp–Moss (KCM) method including its further development, the γ-expansion (GE) method [14], were used. Following a subsequent Monte Carlo simulation, a closer agreement with the original short-range order scattering was achieved using the EPI parameters from the KCM + GE method. Although the inverse Monte Carlo method is approximation free, the closeness of the two states to the $\gamma/(\gamma + \eta)$ phase boundary seems to be crucial. This leads to a too high intensity at the 100 positions (by 0.4 Laue units for ^{58}Ni–5.8 at.% Ti and 1.7 Laue units for ^{58}Ni–9.6 at.% Ti). Both sets of EPI parameters are close to one another, they are dominated by the values of the first two shells ($V_{110} = 39$ meV and $V_{200} = -16$ meV for ^{58}Ni–5.8 at.% Ti, $V_{110} = 43$ meV and $V_{200} = -17$ meV for ^{58}Ni–9.6 at.% Ti).

Static atomic displacements for different alloys are not easily compared as neutron scattering only yields a linear combination of the two independent species-dependent static displacements, e.g. between Ni–Ni pairs, $\langle x^{NiNi}_{lmn} \rangle$, and Ti–Ti pairs, $\langle x^{TiTi}_{lmn} \rangle$, still weighted with the atomic fractions and α_{lmn}, besides the coherent scattering lengths. Fig. 4 shows that the size-effect scattering is larger for the room temperature measurement of ^{58}Ni–5.8 at.% Ti than for the at-temperature measurement of ^{58}Ni–9.6 at.% Ti. Fourier coefficients of the 110, 200 and 220 shells are dominant, while those for the 211 shell are small. The latter, however, is of special interest as a possible indicator of the η phase, since it involves the direction of the Burgers vector $\underline{b} = \langle 112 \rangle a/3$ of the superpartials proposed in a formal

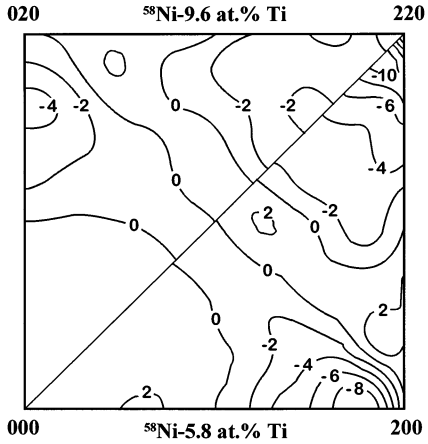

Fig. 4. Recalculated size-effect scattering in 0.1 Laue units for the 001 plane of ^{58}Ni–5.8 at.% Ti and ^{58}Ni–9.6 at.% Ti.

shear model for the $L1_2$ to $D0_{24}$ transformation [15]. Thus, precursors for this phase transformation are neither found in the static atomic displacements nor in the dynamical displacements [9].

4. The metastable γ″ precipitates

The decomposition kinetics of supersaturated solid solutions with (10–12) at.% Ti was followed in situ by small-angle neutron scattering. The initial scattering patterns of states quenched from the γ solid solution were always flat on the two-dimensional detector. As the coherent scattering lengths of Ni and Ti differ in sign, this is a very sensitive indicator of compositional homogeneity. As aging proceeded, the scattering increased, an interference peak evolved and moved to smaller Q. To determine the integrated SANS intensity $\tilde{Q} = \int I(\underline{Q}) d\underline{Q}$, the scattering patterns were averaged over rings of constant Q. The Q-independent scattering contributions (elastic incoherent and 'Laue' scattering) present beside the A/Q^4 term (A = Porod constant) at large Q, were separated to yield the relevant (absolute) scattering intensity $I(\underline{Q})$.

Within the two-phase model of precipitates of Ti fraction c_p embedded in the matrix of Ti fraction c_m, the integrated intensity is given by:

$$\tilde{Q} = (2\pi)^3 (c_p - c_{Ti})(c_{Ti} - c_m)|b_{Ni} - b_{Ti}|^2 / V_{at}^2 \quad (3)$$

where V_{at} is the average atomic volume. Fig. 5 shows the time dependence of the integrated SANS intensity for two alloys. For the alloy with the higher Ti fraction, intermediate plateaus in $\tilde{Q}$ are resolved indicating metastable states. Assuming c_m to be given by the coherent solvus (about 9 at.% Ti [16]), the Ti fraction within the precipitates amounts to about 17 at.% (Fig. 1). This value is close to the metastable miscibility gap suggested by Hashimoto and Tsujimoto [1]. Whether the appearance of the intermediate γ″ state depends on the location of the instability lines introduced by Soffa and Laughlin [2] and estimated from the EPI parameters (Fig. 1), still has to be clarified. The subsequent increase in the integrated intensity with further aging is not related to the appearance of η platelets. Dark-field transmission electron micrographs taken for such states still show exclusively coherent precipitates of cuboidal shape (Fig. 6).

In conclusion, the $L1_2$ type of order of precipitates known for the metastable γ″ and γ′ states is also indicated in the γ solid solution. Its preservation in the $D0_{24}$ structure within the close-packed planes is analogous to the situation in Ag–Al; the site occupa-

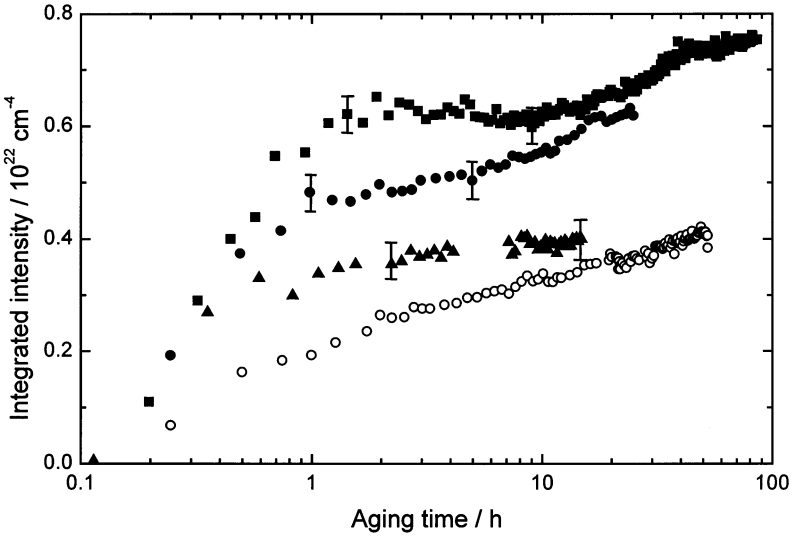

Fig. 5. Integrated SANS intensity $\tilde{Q}$ as a function of aging time for Ni–10.1 at.% Ti at 900 K (open circles) and for Ni–11.3 at.% Ti at 870 K (filled squares), 900 K (filled circles) and 950 K (filled triangles).

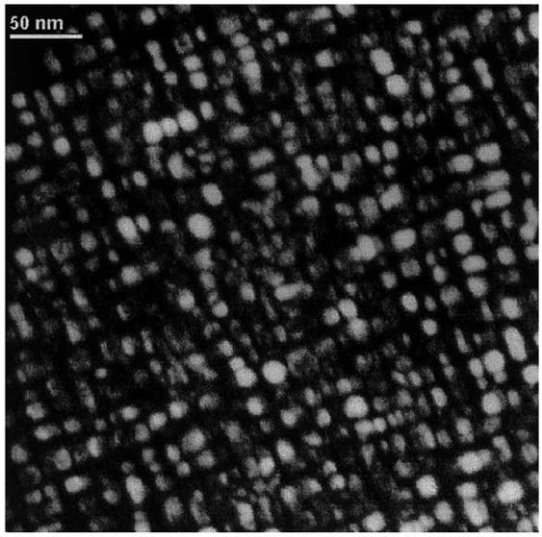

Fig. 6. Dark-field transmission electron micrograph (taken at 160 keV, [001] surface normal, 100 superstructure reflection) of Ni–11.3 at.% Ti aged at 873 K for 96 h.

tion within the close-packed planes of the cubic A_5B structure and the hexagonal 'Neumann' structure proposed as ground states, is also identical [17].

References

[1] K. Hashimoto, T. Tsujimoto, Trans. JIM 19 (1978) 77.
[2] W.A. Soffa, D.E. Laughlin, Acta Metall. 37 (1989) 3019.
[3] A. Cerri, B. Schönfeld, G. Kostorz, Phys. Rev. B42 (1990) 958.
[4] P. Vyskocil, J. Skov Pedersen, G. Kostorz, B. Schönfeld, Acta Mater. 45 (1997) 3311.
[5] G. Kostorz, M. Kompatscher, B. Schönfeld, in: M. Koiwa, K. Otsuka, T. Miyazaki (Eds.), Solid–Solid Phase Transformations '99, Japan Institute of Metals, Sendai, Japan, 1999, p. 305.
[6] M. Kompatscher, B. Schönfeld, H. Heinrich, G. Kostorz, J. Appl. Cryst. 33 (2000) 488.
[7] T.B. Massalski, Binary Alloy Phase Diagrams, vol. 2, ASM International, Materials Park, OH, 1990.
[8] P. Bellen, K.C. Hari Kumar, P. Wollants, Z. Metallkd. 87 (1996) 972.
[9] R. Bucher, B. Schönfeld, G. Kostorz, M. Zolliker, Phys. Stat. Sol. A175 (1999) 527.
[10] G. Kostorz, in: R.W. Cahn, P. Haasen (Eds.), Physical Metallurgy, 4th edn, North-Holland, Amsterdam, 1996, p. 1115.
[11] B. Schönfeld, Prog. Mater. Sci. 44 (1999) 435.
[12] P.C. Clapp, Phys. Rev. B4 (1971) 255.
[13] V. Gerold, J. Kern, Acta Metall. 35 (1987) 393.
[14] I. Tsatskis, in: S.J.L. Billinge, M.F. Thorpe (Eds.), Local Structure from Diffraction, Plenum, New York, 1998, p. 207.
[15] M. Lambrigger, H.A. Calderon, G. Kostorz, Z. Metallkd. 83 (1992) 624.
[16] P.K. Rastogi, A.J. Ardell, Acta Metall. 17 (1969) 595.
[17] S.-Y. Yu, B. Schönfeld, G. Kostorz, in: M. Koiwa, K. Otsuka, T. Miyazaki (Eds.), Solid–Solid Phase Transformations '99, Japan Institute of Metals, Sendai, Japan, 1999, p. 37.